

This is the preprint of the contribution published as:

Zhou, J., Saeidi, N., Wick, L.Y., Kopinke, F.-D., Georgi, A. (2021):

Adsorption of polar and ionic organic compounds on activated carbon: surface chemistry matters

Sci. Total Environ. , art. 148508

The publisher's version is available at:

<http://dx.doi.org/10.1016/j.scitotenv.2021.148508>

**Adsorption of polar and ionic organic compounds on activated carbon:
Surface chemistry matters**

Jieying Zhou^a, Navid Saeidi^a, Lukas Y. Wick^b, Frank-Dieter Kopinke^a, Anett Georgi^{a,*}

^a*Helmholtz Centre for Environmental Research – UFZ, Department of Environmental
Engineering, D-04318 Leipzig, Germany.*

^b*Helmholtz Centre for Environmental Research – UFZ, Department of Environmental
Microbiology, D-04318 Leipzig, Germany*

Corresponding author contact information: Tel.: +49 341 235 1760; Fax: +49 341 235 1471;

E-mail: anett.georgi@ufz.de

Keywords: AC, adsorption processes, surface modification, persistent and mobile organic compounds, water treatment

Abstract

Persistent and mobile organic compounds (PMOCs) are often detected micropollutants in the water cycle, thereby challenging the conventional wastewater and drinking water treatment techniques. Carbon-based adsorbents are often less effective or even unable to remove this class of pollutants. Understanding of PMOC adsorption mechanisms is urgently needed for advanced treatment of PMOC-contaminated water. Here, we investigated the effect of surface modifications of activated carbon felts (ACFs) on the adsorption of six selected PMOCs carrying polar or ionic groups. Among three ACFs, defunctionalized ACF bearing net positive surface charge at neutral pH provides the most versatile sorption efficiency for all studied PMOC types representing neutral, anionic and cationic compounds. Ion exchange capacity giving quantitative information of sorbent surface charges at specified pH is recognized as a frequently underestimated key property for evaluating adsorbents aiming at PMOC adsorption. A most recently developed prediction tool for Freundlich parameters in PMOC adsorption was applied and the prediction results are compared to the experimental data. The comparison demonstrates the so far underestimated importance of the sorbent surface chemistry for PMOC adsorption affinity and capacity. PMOC adsorption mechanisms were additionally investigated by adsorption experiments at various temperatures, pH values and electrolyte concentrations. Exothermic sorption was observed for all sorbate-sorbent pairs. Adsorption is improved for ionic PMOCs on AC carrying sites of the same charge (positive or negative) at increased electrolyte concentration, while not affected for neutral PMOCs unless strong electron donor-acceptor yet weak non-Coulombic interactions exist. Our findings will allow for better design and targeted application of activated carbon-based sorbents in water treatment facilities.

1. Introduction

Almost a half of the European chemicals regulation (REACH) registered organic substances with unique CAS numbers (including predicted hydrolysis products) exhibit highly polar, ionic or ionizable structures (Arp et al., 2017; Arp and Hale, 2019). Among them, the compounds with freshwater half-lives longer than 40 days and soil organic carbon–water distribution coefficients $\log D_{oc} < 4.5$ (at pH = 4–10) are referred to persistent and mobile organic compounds (PMOCs) (Arp et al., 2017). Many of these compounds readily pass the conventional water treatment processes and become increasingly detectable in aquatic environments (Farré et al., 2008; Loos et al., 2013; Reemtsma et al., 2006; Schulze et al., 2019). Although detected in low concentrations (ng/L – $\mu\text{g/L}$), they may recirculate and accumulate in short water cycles (Arp et al., 2017; Teychene et al., 2020), raising considerable toxicological concerns under long-term exposure (Arp et al., 2017; Farré et al., 2008; Fent et al., 2006; Ferrari et al., 2003; Loos et al., 2013; Sinclair and Boxall, 2003; Sophia A and Lima, 2018; Thomaidi et al., 2015).

In wastewater and drinking water treatment plants, adsorption technology is widely used due to its advantages including flexibility in operation mode (batch or continuous processes), operational simplicity, low investment costs and low environmental impact (EPA, 2020; Sophia A and Lima, 2018; Watson, 1999). Activated carbon (AC) materials with specific surface areas $\sim 10^3 \text{ m}^2/\text{g}$ are frequently used as adsorbents. Besides ozonation, AC adsorption is presently the most broadly applied and recommended technique for upgrading wastewater treatment plants (Decrey et al., 2020; Reemtsma et al., 2016).

The appearance of PMOCs in the aquatic environment points to a significant treatment gap in the current wastewater and drinking water purification processes where higher adsorption efficiency of AC adsorbents is urgently called for (Reemtsma et al., 2016). Being structurally different from the conventional nonpolar organic pollutants, PMOCs can interact with the

sorbent surfaces additionally by means of electrostatic interactions, ion exchange, ion bridging, electron donor-acceptor (EDA) interactions and charge-assisted H-bonds (Kah et al., 2017). Previous studies have shed light on the diverse effects of surface chemistry of AC materials on adsorption of PMOCs. For instance, it was discovered that defunctionalization of commercial activated carbon felts (ACFs) to remove oxygen-containing functional groups significantly fostered the adsorption of perfluorooctanoic acid (PFOA, pK_a between 0 and 1 (Goss, 2008)) and perfluorooctanesulfonic acid (PFOS, $pK_a = -3.27$ (Brooke et al., 2004)) yet less strongly for *n*-octanoic acid ($pK_a = 4.9$ (Wellen et al., 2017)). Nevertheless, an in-depth understanding of the links between AC properties and PMOCs adsorption is still missing to date (ECETOC, 2013; Mailler et al., 2016).

Given the large variety of chemical PMOC structures, generic mechanistic understanding and predictive modeling approaches of PMOC sorption on carbonaceous materials are needed for targeted sorbent design (Kah et al., 2017; Schulze et al., 2019). Polyparameter linear free energy relationships (pp-LFERs) have long been successfully applied to predict partitioning and (under certain conditions) also adsorption processes of *non-ionic* organic compounds (Endo and Goss, 2014). However, prediction tools for sorption of *polar and ionic* organic compounds onto activated carbon and related sorbents from aqueous systems were much less focused on and only started to emerge recently (Sigmund et al., 2020b). These model approaches are either based on LFERs (Zhao et al., 2019), a combination of neural networks (NN) and pp-LFERs (Zhang et al., 2020) or on NN solely (Sigmund et al., 2020b). All these models use Abraham descriptors of the sorbates as input parameters, i.e. E (excess molar refraction), S (effective dipolarity/polarizability), A (hydrogen bond acidity), B (hydrogen bond basicity) and V (characteristic McGowan volume, $\text{cm}^3/\text{mol}/100$). The model only based on LFER by Zhao et al. (2019) also included the specific ionic descriptors J^+ and J^- for columbic interactions (Abraham and Zhao, 2004), yet neglected the influence of sorbent textural and chemical

properties on PMOC adsorption. The model established by Zhang et al. (2020) by contrast considers pore-filling and hydrophobic effects as adsorption drivers and, hence, includes total pore volume (V_t) and BET-derived specific surface area (S_{BET}) as sorbent-related input parameters. These two sorbent-parameters are, however, highly correlated (Sigmund et al., 2020a). This model is predominantly trained with sorption data on carbonaceous sorbents with $S_{\text{BET}} \geq 400 \text{ m}^2/\text{g}$. Another most recently developed model by Sigmund et al. (2020b) is based on the sorbent's S_{BET} and elemental composition (C wt%, H/C and O/C molar ratios) combined with the sorbates' $\log D$, A^- % or B^+ % (pH-dependent percentage of anionic or cationic species, respectively). Although many data on the elemental composition of C-based adsorbents of moderate carbonization degree exist (e.g. for biochars), they are heavily missing for ACs applied in sorption studies. As a result, only 55 out of 330 items in the training-set for anionic and polar organic compounds used in (Sigmund et al., 2020b) exhibit $S_{\text{BET}} \geq 400 \text{ m}^2/\text{g}$. While all three prediction tools deepen our understanding of PMOC sorption on carbon-based materials, they are all affected by limitations in appropriate experimental literature data for model training. Data shortages include (i) detailed characterization of AC sorbents and their ion exchange capacities (Sigmund et al., 2020b), (ii) high-quality adsorption isotherm data, and (iii) lack of adsorption studies on cationic organic compounds (“small and noisy data set” (Sigmund et al., 2020b)).

In order to advance the presently limited knowledge on correlations between PMOC adsorption and AC properties, we here studied for the first time the adsorption of six environmentally relevant PMOCs on three types of ACFs of high specific surface area ($S_{\text{BET}} = 1100\text{--}1500 \text{ m}^2/\text{g}$) and similar porous structures yet distinct surface functionalities. The PMOC adsorbates consist of three positively charged compounds (benzyltrimethylammonium (BTMA^+), benzyltriethylammonium (BTEA^+), tetrapropyl-ammonium (TPA^+)), an organic anion (*p*-toluenesulfonate, $p\text{-TsO}^-$, acid form with $\text{p}K_a < -1$ (Guthrie, 1978; Sergeant and Dempsey,

1979)), and two neutral molecules (at pH 7; methyl-*tert*-butyl ether (MTBE), *p*-toluenesulfonamide (*p*-TSA, $pK_a = 10.5$ (Atwood and Steed, 2004))). According to Schulze et al. (2018), MTBE, *p*-TsO⁻, and BTMA⁺ have a high environmental emission potential, i.e. were ranked 3rd, 50th, and 313th out of 936 REACH registered PMOCs (Schulze et al., 2018). Additionally, MTBE, *p*-TsO⁻, and BTMA⁺ are among the most persistent and mobile aquatic PMOCs with freshwater half-lives of >60 d, log D_{oc} of <1 at pH = 4–10 and a water solubility >10 g/L (Arp et al., 2017). Despite the high environmental relevance, very limited adsorption studies on such PMOCs were performed and yet, except for MTBE adsorption on 15 different AC materials reported by Li et al. (2002), most previous studies did not focus on the impact of the sorbent surface chemistry (Davarpanah et al., 2015; Duman and Ayranci, 2010; Qi et al., 2013; Tamai et al., 2004; Wu et al., 2011). Herein, to analyze effects of AC surface properties on the PMOCs' sorption affinity and capacity, isotherms of individual sorbate-sorbent pairs were measured at different temperature, electrolyte concentration and pH conditions. To understand the role of AC surface chemistry for PMOC adsorption we further fitted our data with Freundlich and Langmuir equations and compared them to results predicted by the model suggested by Sigmund et al. (2020b).

2. Experimental section

2.1 Chemicals

p -TsO⁻ (commercially available in form of C₇H₈O₃S·H₂O, > 98.5%) and BTMA hydroxide (C₁₀H₁₇NO, 20 w/w% aq.) were obtained from Alfa Aesar. p -TSA (C₇H₉NO₂S, ≥99%) and TPA hydroxide (C₁₂H₂₉NO, 1.0 M aq.) were purchased from Sigma-Aldrich. MTBE (C₅H₁₂O, >99%) and BTEA hydroxide (C₁₃H₂₃NO, 10 w/w% aq.) were acquired from Fluka Analytical and abcr GmbH, respectively. Selected sorbate properties are listed in Table S1. Ethanol (EtOH, ≥99.9%), HNO₃ (65%), HCl (37%), NaOH (99%), KCl (>99%), NaNO₃ (>99%), Na₂SO₄ (99%), CuSO₄·5H₂O (>99%), citric acid monohydrate (C₆H₈O₇·H₂O, >99%) and the ammonia solution (25 w/w% aq.) were purchased from Merck. Methanol (>99.95%) and *i*-propanol (≥99.9%) were obtained from Th.Geyer. Oxalic acid bis(cyclohexylidene hydrazide) (Cuprizone, C₁₄H₂₂N₄O₂, > 98%) and ammonium acetate (C₂H₇NO₂, ≥98.0%) were purchased from Bernd Kraft GmbH. Deionized water was used to prepare all solutions.

2.2 Materials

Actitex®-FC1001 (Jacobi CARBONS, ACF₁₀ in short, 30 cm²) was washed with *i*-propanol (60 mL) and five times with H₂O (60 mL, shaking at 120 rpm, 30 min) followed by air-drying (80°C, overnight) before use or further treatment. The oxidized sample (OxACF₁₀) was prepared by stirring ACF₁₀ (1.1 g) in HNO₃ (5 M, 130 mL) at 95°C for 6 h. The as-treated sample was then washed five times with H₂O (shaking at 120 rpm, 30 min) until pH reached approx. 6 and then air-dried (50°C, overnight). The defunctionalized sample (DeACF₁₀) was prepared by treating ACF₁₀ in a quartz tubular oven at 900°C under H₂ atmosphere for 2 h (heating rate: 150 K/min, starting from 20°C, gas flow rate: 40 mL/min). Before heating, the

oven containing the sample was purged with N₂ for 30 min and then with H₂ for another 30 min. After heating, the oven was cooled automatically to 100°C in H₂, then to 20°C in N₂.

2.3 Material characterization

The specific surface area (S_{BET}) of the sorbents was measured with the BET method (N₂ at 77 K) using BELSORP MINI (BEL Japen, Ltd.) with a sample pretreatment at 100°C. The mesopore size distribution ($\varnothing > 2$ nm) was characterized by the BJH method. The size distribution of the micropores ($\varnothing < 2$ nm) was determined using a magnetic suspension balance (Rubotherm GmbH) by means of CO₂ adsorption at 0°C and analysed by NLDFT fitting from the software Pore analyser (Porotec GmbH). The point of zero net proton charge (pH_{PZC}) of the ACF samples was determined as reported (Babić et al., 1999). Cation and anion exchange capacities (CEC and AEC) were determined as described earlier (Saeidi et al., 2020a; Zelazny et al., 1996). The detailed procedures for pH_{PZC} and CEC/AEC determination are given in SI. Elemental analysis was performed using a CHN analyser (LECO TruSpec CHN). The oxygen contents of the samples were calculated from the mass balance $\text{O wt\%} = 100\% - \text{C wt\%} - \text{H wt\%} - \text{N wt\%} - \text{ash wt\%}$. The ash content was determined gravimetrically as residue after burning the sample at 750°C in oxygen. Temperature-programmed desorption (TPD) results were recorded on a BELCAT-B chemisorption analyser (BEL Japan Ltd.) coupled with an Infracal detector (SAXON Junkalor) for CO and CO₂ detection. The ACFs were first pre-treated at 150°C for 30 min in an argon atmosphere (50 mL/min), then heated up from 150°C to 1100°C with a heating rate of 10 K/min. X-ray photoelectron spectroscopy (XPS) measurements were performed by an Axis Ultra photoelectron spectrometer (Kratos Analytical Ltd.) using monochromatized Al K α radiation ($h\nu = 1486.6$ eV). For binding energy (BE) determination, the main component of the C1s signal at 284.8 eV was employed as reference. Peak

deconvolution was performed with CasaXPS (<http://www.casaxps.com/>) by applying a Shirley background and sums of Gaussian and Lorentzian functions for the fitting. The Attenuated total reflection (ATR)-FTIR was performed on a Nicolet iS50R FR-IR device (ThermoFischer). The morphology of ACFs was characterized using scanning electron microscopy (SEM) (Zeiss Merlin VP Compact).

2.4 Adsorption experiments

0.1–4.0 g/L ACFs were shaken (120 rpm) for 24–48 h in aqueous Na₂SO₄ solution (1–100 mM, 8–10 mL) followed by pH adjustment with 0.1 M NaOH and/or H₂SO₄ solutions to desired values. Such pre-wetting step allows background solution to penetrate the inner pores, making them readily accessible for dissolved sorbates (Duman and Ayranci, 2010). Then, stock solutions containing individual sorbate compounds (1–3 g/L) pre-neutralized to pH 7 were added to the ACF-containing batches to reach desired initial concentrations (2.5 – 80 mg/L). After shaking overnight at the selected temperatures (20°C, 40°C, 55°C, and 70°C, 400 rpm with LLG-uniTHERMIX 2 pro), the pH values of the suspensions were adjusted back to desired values. Temperature dependence was measured for exploring the impact of entropy and enthalpy effects in the adsorption processes. For samples containing nonionic MTBE, the pH-adjustment during the adsorption process was abandoned. Also, gas-liquid volume ratios <1:5 were set so that MTBE loss into the gas phase was negligible. After 48 h-adsorption at the selected temperature, samples were taken and filtered with Whatman® syringe filters (0.45 µm, PTFE), concentrated by evaporation of water under N₂ or diluted when necessary, and used for concentration measurement. The final pH values were detected in the range (± 0.5) close to the desired values.

The single-point adsorption coefficient K_d (L/m^2) indicating the adsorption affinity of the sorbent towards the sorbate at a given condition was calculated as

$$K_d = \frac{q_e}{c_e} \quad (1)$$

where q_e ($\mu\text{mol}/m^2$) related to sorbent's S_{BET} is the sorbent loading and c_e ($\mu\text{mol}/L$) the concentration of dissolved solute in the aqueous phase at the adsorption equilibrium.

The adsorption isotherms of sorbate-sorbent pairs were fitted with linearized forms of Freundlich (Eq. 2) and Langmuir equations (Eq. 3) expressed as follows,

$$\log q_e = n \cdot \log c_e + \log K_F \quad (2)$$

where n is the dimensionless Freundlich exponent and K_F ($(\mu\text{mol}/m^2)/(\mu\text{mol}/L)^n$) is the Freundlich constant (Aljerf, 2018). In addition, K_F in unit of $(\mu\text{g}/\text{kg})/(\mu\text{g}/L)^n$ is derived from fittings using q_e ($\mu\text{g}/\text{kg}$) related to adsorbent mass and c_e ($\mu\text{g}/L$) to compare with the model predictions in Section 3.2.4. Logarithms of parameters which carry units are to be understood as numbers after dividing by these units.

$$\frac{c_e}{q_e} = \frac{c_e}{q_{\max}} + \frac{1}{q_{\max}K_L} \quad (3)$$

where q_{\max} ($\mu\text{mol}/m^2$) is the maximal (monolayer) sorbent loading and K_L ($L/\mu\text{mol}$) the Langmuir constant. Both K_F and K_L are related to the adsorption affinity of the sorbent towards the selected sorbate while q_{\max} represents the adsorption capacity. $n \rightarrow 1$ indicates a more homogenous distribution of sorption sites on sorbent surface (Delpeux-Ouldriane et al., 2015; Li et al., 2002).

2.5 Analytical methods

Aliquots of aqueous samples were taken using a syringes equipped with Whatman® (0.45 µm, PTFE) filters before being measured. The analysis of p -TsO⁻ and TPA⁺ was accomplished by a liquid chromatography equipment coupled with a photo diode array UV/VIS detector and single-stage mass spectrometer (MS) with electrospray ionization (LC-MS2020, SHIMADZU Corporation). UV/VIS detection was applied for p -TsO⁻ ($\lambda = 220$ nm) and the MS detector operated in selected ion monitoring (SIM) mode with $m/z = 186$ amu was used for TPA⁺. The concentrations of p -TSA were analysed by gas chromatography–mass spectrometry (SHIMADZU GC–MS 2010) in SIM mode ($m/z = 171$ amu) after solvent extraction (for details see SI part). MTBE concentrations were determined by Headspace-GC–MS analysis using a SHIMADZU AOC-5000 Plus autosampler coupled to the above mentioned GC–MS operated in SIM mode ($m/z = 73$ amu). The concentrations of dissolved BTMA⁺ and BTEA⁺ were both measured by UV/VIS spectrometry (SHIMADZU UVmini-1240) at $\lambda = 207$ nm. Corresponding blank samples without analytes were prepared for correcting the baseline. To measure the Cu²⁺ concentrations, 1–6 mL aliquots were added to a combination of 1 mL cuprizone solution (0.5 wt% in EtOH:H₂O = 1:1 v/v) and 1 mL triammonium citrate-ammonia buffer ((NH₄)₃C₆H₅O₇–NH₃, pH = 9) solution to form the copper-cuprizone complex absorbing intensively at 595 nm (Messori et al., 2007). The mixture was shaken for 30 min (120 rpm) in darkness before diluted to the concentration range 0.1–2 mg/L and analysed by UV/VIS spectrometry. More detailed information of the measurements is given in the SI part.

3. Results and discussion

3.1 Characterization of ACFs

Derived from a commercially available ACF₁₀, two surface-modified ACFs were prepared to provide distinct sorbent properties for adsorption of selected polar organic compounds. All three ACFs were carefully characterized for their bulk chemical composition, surface functionalities and pore structures.

Elemental analyses were performed for all studied ACF types with results listed in Table 1. HNO₃ oxidation of ACF resulted a 1.8-fold increased O content (18.1 wt%) of OxACF₁₀ relative to untreated ACF₁₀ (9.9 wt%) while annealing of the original ACF₁₀ in H₂ flow at 900°C for 2 h resulted in a significant reduction in the O content (4.3 wt%) of DeACF₁₀. TPD was performed to further characterize the O-containing functional groups (Fig. S1). Observed peaks at $T \approx 800$ K, 1000 K and 1100–1200 K in the CO release profiles can be assigned to the destruction of aliphatic hydroxyl, phenolic hydroxyl and carbonyl groups, respectively (Vogel et al., 2019). In CO₂ release profiles, the peak around 500 K may refer to the decomposition of carboxylic or anhydride groups (Vogel et al., 2019; Zhou et al., 2007) while CO₂ release at higher temperatures (700–1000 K) is likely to be derived from lactone groups (Zhou et al., 2007). The ATR-FTIR spectra (Fig. S2) also confirm the origins of O-containing functional groups on OxACF₁₀. XPS high resolution C1s spectra (Fig. S3) show an increased peak intensity relating to $\pi \rightarrow \pi^*$ shake-up which implies higher contents of sp² C and, accordingly, more hydrophobic surfaces in the order of OxACF₁₀ < ACF₁₀ < DeACF₁₀.

To quantify charged sites on ACF surfaces, the ion exchange capacities towards inorganic cations and anions were characterized at circumneutral pH. Cation and anion exchange capacities (CEC and AEC, respectively) give quantitative information on surface charge densities of AC at a specified relevant pH. These are favoured compared to other parameters

used for describing AC surface chemistry, such as O-content which does not contain information on the speciation of the O-containing groups or point-of-zero charge (pH_{PZC}) which only gives qualitative information on the predominant charge at $\text{pH} \neq \text{pH}_{\text{PZC}}$ for heterogeneous adsorbent surfaces. Distinct charge densities of the three ACF surfaces were found (Table 1). Differences in ion exchange capacities were mainly attributed to O contents of the samples due to the quasi absence of N in the ACFs (Yang, 2019). Generally, higher CEC were found in ACFs carrying more O-containing functional groups and, hence, more negatively charged sites at circumneutral pH. In contrast, higher AEC was found for oxygen-poor DeACF₁₀. As supported by the XPS spectra (Fig. S11), DeACF₁₀ surface is rather rich in aromatic regions free of O-containing functional groups, and possess highly delocalized π -electrons. Such structures are prone to adsorb protons and form positively charged sites (Saeidi et al., 2020a). The increase of the pH_{PZC} of the ACFs was in the order of OxACF₁₀ < ACF₁₀ < DeACF₁₀ and relates to the order of the ACF ion exchange capacities. The CEC of the sorbents also reflects well their capacity to retain Cu^{2+} (Table S2, Fig. S4).

Analysis of the textural properties (Table 2) revealed for all three ACF high specific surface areas ($> 1000 \text{ m}^2/\text{g}$) as obtained from N_2 BET analyses (S_{BET}) suggesting high PMOC sorption capacities. 93% of S_{BET} is maintained for DeACF₁₀ after thermal treatment in H_2 at 900°C , whereas a 27% loss in S_{BET} was found for OxACF₁₀ after oxidizing with hot HNO_3 solution. The N_2 adsorption-desorption isotherms of all ACFs (Fig. S5a) resemble the IUPAC Type I isotherm (Sing et al., 1985) typically observed for microporous AC materials. The narrow hysteresis loops further indicate a predominance of micropores in all ACFs (Allothman, 2012; Lee et al., 2013; Zhao et al., 2016). Analysis of the pore volume distributions of the ACFs (Fig. S5b) reveals that oxidation of the ACF₁₀ led to a decrease in the fraction of micropores ($\text{\AA} < 2 \text{ nm}$) likely due to pore blocking by O-containing surface functional groups (Bayram and

Ayranci, 2011; Hotová et al., 2020), and accordingly a reduced S_{BET} . The morphology of the three ACFs is shown in SEM images (Fig. S6).

3.2 PMOCs adsorption

3.2.1 Adsorption affinities and capacities of ACFs towards PMOCs

Adsorption isotherms in 10 mM Na_2SO_4 solution at pH 7 (Fig. S7) were determined to quantify PMOC adsorption affinities (K_d) and capacities (q_{max}) to the ACFs. All isotherms were fitted by both the Freundlich equation (Eq. 2) in the low c_e range (i.e. below saturation loading, Fig. S8) and by Langmuir equation (Eq. 3) in the whole data range (Fig. S9) as summarized in Table 3. Log K_d for all sorbate-sorbent pairs at $c_e = 20 \mu\text{mol/L}$ (Fig. 1) were calculated from the Freundlich parameters by $K_d = c_e^{n-1} \cdot K_F$ (cf. Eqs. 1 & 2).

As described in Section 3.1, all three ACF sorbents studied carry porous structures dominated by micropores. Based on the characterization results given in Table 2, the total pore volumes on unit specific surface ($(0.45 \pm 0.07) \text{ mm}^3/\text{m}^2$) are comparable for all three ACFs. Although the pore size distribution differs for the three ACF types, these differences should not result in large varieties in adsorption capacities towards target PMOCs (Table 3) due to the only minor to moderate pore filling extents as elucidated below. For instance, TPA^+ exhibits the largest van der Waals molecular volume ($\approx 139.8 \text{ cm}^3/\text{mol}$) and molecule size (0.63–0.97 nm (Tamai et al., 2004)) of all tested PMOCs. However, TPA^+ exhibited higher sorption to OxACF_{10} ($q_{\text{max}} = 0.18 \mu\text{mol}/\text{m}^2$) than to DeACF_{10} ($q_{\text{max}} = 0.13 \mu\text{mol}/\text{m}^2$) although the $V_{\phi \geq 1 \text{ nm}}$ of OxACF_{10} was found to be about 50% lower than in DeACF_{10} (Table 2). With a simplified assumption that TPA^+ molecules solely enter pores of $\phi \geq 1 \text{ nm}$, only about 7.9% of pores with $\phi \geq 1 \text{ nm}$ of OxACF_{10} would be occupied (for calculation cf. SI). Similarly, we estimated the maximal pore filling extents of all sorbates in pores with $\phi \geq 1 \text{ nm}$ of OxACF_{10} , ACF_{10} and DeACF_{10} (Table S3).

As-obtained data show that the pores were occupied between 0.7 and 32%, suggesting that the sorbent pore volumes may not be the limiting factor for PMOC sorption to the ACFs.

K_d and q_{max} values propose distinct PMOC sorption to the ACFs; in particular for anionic p -TsO⁻ and neutral p -TSA and MTBE. For instance, p -TSA and MTBE adsorption affinities ($\log K_d$; Fig. 1) and the maximum adsorption capacities (q_{max} ; Table 3) follow the order of DeACF₁₀ > ACF₁₀ > OxACF₁₀. Two factors may explain these findings: (i) increasing polarity of the sorbent surfaces due to oxidation penalizes the organic sorbates in the competition with water molecules for adsorption. (ii) Additional EDA interactions between the lone electron pairs of the p -TSA and MTBE heteroatoms and the protonated DeACF₁₀ surface as had been previously reported for MTBE (Li et al., 2002). p -TSA, however, was adsorbed with higher sorption affinities on all ACFs than MTBE despite its lower $\log D$ which shall indicate a weaker hydrophobic effect (Table S1, Kah et al., 2017). This is likely due to additional π - π interactions (Wu et al., 2011) of p -TSA. Furthermore, charge-assisted hydrogen bonds ((\pm) CAHB, being relevant at $\Delta pK_a < 5$ (Li et al., 2013; Teixidó et al., 2011)) between p -TSA ($pK_a = 10.5$) and ACF surfaces (carboxyl groups with $pK_a = 3-6$ (Strelko et al., 2002) and phenolic groups with $pK_a = 8-10$ (Xiao and Pignatello, 2016)) might contribute as well. However, the strong increase in K_d and q_{max} of p -TSA upon defunctionalization of the carbon surface rather speaks for a minor contribution of (\pm) CAHB to its overall sorption.

Adsorption of charged PMOCs requires charge compensation either by oppositely charged sites on adsorbent surface (ion exchange) or co-adsorption of charge-balancing counter ions from the electrolyte solution (Kah et al., 2017; Schwarzenbach et al., 1993). As a measure of the surface charging state of AC surfaces, CEC and AEC values are highly relevant and recommended to be measured, yet largely missing in the literature pool (Kah et al., 2017; Sigmund et al., 2020b). Different to the pH_{PZC} which only gives qualitative information on the net surface charge, CEC and AEC provide quantitative information on the content of negatively

and positively charged surface sites, respectively, at a certain pH value. Since the CEC of the ACFs was $\text{OxACF}_{10} > \text{ACF}_{10} \gg \text{DeACF}_{10}$ (Table 1), better sorption of the cationic PMOCs to OxACF_{10} than to DeACF_{10} could be expected. However, rather similar q_{\max} and $\log K_d$ of TPA^+ , BTMA^+ and BTEA^+ were found for all ACFs (Table 3, Fig. 1) despite the low CEC of the defunctionalized and net positively charged DeACF_{10} surface. Only for BTMA^+ , i.e., the smallest cationic PMOC under study, slightly higher $\log K_d$ and q_{\max} were observed on OxACF_{10} . This points at the relevance of hydrophobicity as a driving force for sorption and may also explain why adsorption capacities of TPA^+ , BTMA^+ and BTEA^+ ($\geq 0.1 \mu\text{mol}/\text{m}^2$) were higher than the CECs of oxygen-poorer ACF_{10} and DeACF_{10} . Also, cation- π EDA interactions might cause additional promoting effects in the adsorption of cationic PMOCs on AC surfaces containing a higher density of π systems (Kah et al., 2017). On the contrary, the q_{\max} of the cationic PMOCs was 50–80% lower than the CEC of OxACF_{10} following the order of $\text{TPA}^+ < \text{BTEA}^+ < \text{BTMA}^+$ ($< \text{Cu}^{2+}$ that accounted for 87% of CEC, cf. Fig. S4, Table S2). The high q_{\max} of cationic PMOCs beyond sorbents' CECs suggest a strong contribution of hydrophobic effects, i.e. the combination of van der Waals forces and solvophobic effects, to the overall sorption due to the relatively bulky non-polar parts in their molecule structure. Such interactions could even overcompensate the net negative charge effects of ACF_{10} surface, as has been described for sorption of alkyl ammonium cations of varying chain lengths to inorganic sorbents (Schwarzenbach et al., 1993). So far, however, systematic studies on similar effects on PMOC adsorption to AC materials are missing. Our results suggest that the reversal of sorbent surface net charge by adsorption of PMOCs depends on the AC surface chemistry: cationic PMOCs can be more easily accommodated beyond sorbents' CECs as found for hydrophobic ACF_{10} and DeACF_{10} , but not for hydrophilic OxACF_{10} . One possible reason for the unexpectedly weak charge effects with cationic sorbates might be the shielding of the positive charge by four more or less bulky substituents, which may prevent a close approach of the N atom to negatively charged surface sites. Anionic sorbates such as $p\text{-TsO}^-$ are not affected in a similar way.

Contrary to the cationic PMOCs, the q_{\max} of negatively charged $p\text{-TsO}^-$ to all ACFs was larger than the sorbents' AECs (Tables 1 & 3) again indicating a superposition of non-Coulombic (hydrophobic) and anion exchange interactions between $p\text{-TsO}^-$ and ACF surfaces. The q_{\max} decreases in the order of $\text{DeACF}_{10} > \text{ACF}_{10} \gg \text{OxACF}_{10}$ (Table 3) and reflects the simultaneous decrease in hydrophobicity and increased number of repulsive negatively charged sites (higher CEC) of OxACF_{10} surface. K_d and q_{\max} of $p\text{-TsO}^-$, however, were significantly lower than of its uncharged derivative $p\text{-TSA}$ (Fig. 1, Table 3) and exhibited more pronounced differences for the differently treated ACFs. This suggests a minor contribution of negative (-) CAHB between $p\text{-TsO}^-$ ($\text{p}K_a = -1.3$) and the carboxyl groups of OxACF_{10} ($\text{p}K_a = 3\text{--}6$) which should otherwise promote the adsorption, and emphasizes the combination of electrostatic and hydrophobic effects as drivers for the sorption of anionic PMOCs. Our findings support recent studies on the sorption trends of anionic per- and polyfluoroalkyl substances (PFAS) (Saeidi et al., 2020a; Zhi and Liu, 2016).

3.2.2 Effect of temperature on adsorption of selected PMOCs

To separate enthalpic and entropic contributions of adsorption, adsorption experiments at different temperatures were performed for TPA^+ , BTMA^+ , $p\text{-TsO}^-$ and $p\text{-TSA}$ and interpreted using a modified van't Hoff equation. The van't Hoff equation (Liu, 2009) links K_{ads} as adsorption equilibrium constant with ΔH_{ads} and ΔS_{ads} as adsorption enthalpy and entropy.

$$\ln K_{\text{ads}} = -\frac{\Delta H_{\text{ads}}}{RT} + \frac{\Delta S_{\text{ads}}}{R} \quad (4)$$

Note that there is an ongoing debate on the correct equilibrium constants to be applied in Eq. 4 for adsorption to solid surfaces (which in principle should be unit-free) (Liu, 2009; Tran et al., 2017). However, it becomes insignificant when aiming at values for adsorption *enthalpy* only.

Thus, we apply a simplified approach, replacing K_{ads} by K_{d} , i.e., the single-point adsorption coefficient in the low sorbent loading range ($q \ll q_{\text{max}}$) to give a modified van't Hoff equation. We consider the derived adsorption enthalpies ($\Delta H_{\text{ads}} = -R \cdot d(\ln K_{\text{d}})/d(1/T)$) as 'apparent' ones, being aware of the limited thermodynamic significance of these values. The calculated values are in the range from $\Delta H_{\text{ads}} = 0$ for adsorption of TPA^+ on OxACF_{10} to -38 kJ/mol for adsorption of $p\text{-TsO}^-$ on DeACF_{10} .

Exothermic sorption was observed for all sorbate-sorbent pairs, with less steep slopes (i.e. less exothermic adsorption) for adsorption to OxACF_{10} than to DeACF_{10} (Fig. 2). Especially, adsorption of cationic TPA^+ and BTMA^+ on OxACF_{10} was found to be quasi thermoneutral. Although these sorbates should experience improved electrostatic attraction with the oxidized carbon surface, sacrificed non-Coulombic interactions on the more hydrophilic sorbent took over. Our findings are in accordance with previous results (Duman and Ayranci, 2010) which showed that adsorption of BTMA^+ and BTEA^+ onto microporous activated carbon cloth was dominated by hydrophobic effects. Entropy seems to be an important driving force for adsorption of the organic cations to the oxidized ACF surface, as most obvious for BTMA^+ where OxACF_{10} shows the lowest slope (lowest ΔH_{ads}) but still highest K_{d} .

Defunctionalization of the ACF generally had minor impacts on the slopes of van't Hoff plots for neutral and cationic PMOCs, yet clearly enhanced the ΔH_{ads} of $p\text{-TsO}^-$. Here, the superposition of improved van der Waals forces, $\pi\text{-}\pi$ and $n\text{-}\pi$ EDA interactions and attractive Coulombic interactions (with protonated π -electron systems) leads to a more exothermic process.

3.2.3 Effect of the ionic strength and pH on adsorption

Ionic strength (IS): applying background electrolyte (Na_2SO_4) with increasing concentrations from 1 mM to 100 mM may influence adsorption of polar and ionic organic compounds by: (i) increased competition for sorption sites by inorganic ions (Kah et al., 2017; Saeidi et al., 2020a), (ii) higher shielding of the sorbent's ion exchange sites due to a compressed electric double layer (EDL) (Brown et al., 2016), and (iii) increased chemical activity of dissolved sorbates by possible salting-out effect (Xiao et al., 2005). As salting-out effects were estimated to cause effects on $\log K_d$ of $< \pm 0.02$ (Schwarzenbach et al., 1993), they are considered negligible for our interpretation and thus are not further considered.

As shown in Fig. 3, poor influence of the salt concentration on $\log K_d$ of *p*-TSA adsorption for any of the ACF was found. This indicates that the strong *p*-TSA adsorption to ACF is mainly driven by non-Coulombic interactions. In contrast, K_d of MTBE on DeACF₁₀ decreased slightly at increasing ionic strengths. Contrary to likewise neutral *p*-TSA, MTBE has no π -electron system to interact with the ACF surface, and the EDA interactions may be hindered either by competitive sorption of SO_4^{2-} or increased shielding of sorption sites. On OxACF₁₀, increasing IS suppressed adsorption of cationic TPA⁺ and BTMA⁺, whereas the anionic *p*-TsO⁻ adsorbed more strongly. These opposite effects can be explained by the same mechanism: joint effect of EDL compression and competing Na⁺ adsorption at the negatively charged OxACF₁₀ surface aroused a weakening of attractive or repulsive electrostatic interactions for cationic and anionic PMOCs, respectively. Similar reasons account for the changes in $\log K_d$ on DeACF₁₀ for charged PMOCs upon IS change (Saeidi et al., 2020a).

The effect of solution pH (at 4, 7 and 9) on the adsorption of selected PMOCs on OxACF₁₀ and DeACF₁₀ is shown in Fig. S10. Decreasing pH from 9 to 4 moderately reduced the adsorption of TPA⁺ and BTMA⁺ on OxACF₁₀ (Fig. S10a). Since pH_{PZC} of OxACF₁₀ is 2.4, the sorbent

surface keeps a negative net charge at pH 4 while the density of negatively charged surface sites increases at higher pH, which clearly benefits the uptake of the cationic PMOCs. Accordingly, the adsorption affinity of p -TsO⁻ on DeACF₁₀ ($pH_{PZC} = 10.2$) increases when decreasing pH from 9 to 4 due to enhanced electrostatic interactions (Fig. S10b). In comparison, no change in $\log K_d$ in the adsorption of neutral p -TSA on DeACF₁₀ was observed at different pH values as expected. The effect of a broader pH range on adsorption of especially weak organic acids and bases was reported to be studied using the bell-shape relationship (Xiao and Pignatello, 2014).

In summary, increases in IS improved adsorption if solutes and net charges of the sorbent surface were of the same sign (positive or negative), while increased IS hindered adsorption if charges were of opposite signs. IS effects on neutral compounds were found only in case of strong EDA yet weak non-Coulombic interactions.

3.2.4 Comparison of experimental data with model predictions

Our experimental PMOC sorption data were compared to model predictions (Sigmund et al., 2020b) adapted for the adsorption of polar organic compounds to carbonaceous materials. As Abraham parameters of ionic compounds are poorly accessible, the comparison was done for MTBE, p -TsO⁻ and p -TSA with Abraham parameters (of their neutral forms) available from the UFZ LSER database (Ulrich et al., 2017) as also proposed by Sigmund et al. (2020b). We further included previously published data on octanoic acid (OCA, $pK_a = 4.9$ (Wellen et al., 2017)) (Saeidi et al., 2020b) and MTBE adsorption (Li et al., 2002). Fig. 4 shows the comparison of $\log K_F$ and n as these two Freundlich parameters are separately predicted for each sorbate-sorbent pair by Sigmund et al. (2020b).

Generally, Fig. 4 reveals higher predicted $\log K_F$ coupled with lower predicted n than experimental-derived ones. In a few cases, for instance among the 17 sets of MTBE adsorption

data compared, the most successful matches were found on AW10 carbon series (incl. oxidized OAW10, H₂-treated HAW10, NH₃-treated AAW10 and pristine AW10 reported in (Li et al., 2002)) carrying $S_{\text{BET}} < 850 \text{ m}^2/\text{g}$ (Fig. 4, SI S4 and SI Excel-file). In contrast, unreasonably high $\log K_{\text{F, pre}} > \log K_{\text{F, exp}} + 1$ were observed on other AC-based sorbents carrying $S_{\text{BET}} > 1100 \text{ m}^2/\text{g}$ (cf. SI S4). The observed mismatch may be explained by the fact that the model was trained heavily with biochar sorbents of relatively low S_{BET} (83% datasets with $S_{\text{BET}} < 400 \text{ m}^2/\text{g}$) as datasets with well characterized AC carrying high S_{BET} are often hard to find in the literature. As S_{BET} was found to be the key property among all 12 input parameters to predict K_{F} and n for anionic and neutral PMOCs according to Sigmund et al. (2020b), results in Fig. 4 suggest that further model training involving well-characterized AC materials of high S_{BET} is needed for successful prediction of PMOC in large-scale water treatment facilities.

Next, we tested if the model allows predicting the effect of changes of ACF's surface chemistry on PMOC adsorption. Although predicted and experimental $\log K_{\text{d}}$ values for adsorption of p -TsO⁻ to ACF₁₀ and p -TSA to ACF₁₀ and DeACF₁₀ were comparable (Fig. 5), the model generally failed to predict the poorer adsorption of PMOCs to ACFs with higher O-contents (i.e. ACFs of more elevated CEC and higher negative surface charge densities at neutral pH). This suggests that sorbent surface chemistry impacts may need to be better considered by the model. As proposed by Sigmund et al. (2020b), model improvements may implement EDA and electrostatic interactions between sorbents and sorbates and, hence, also consider parameters describing sorbent surface charge. Although ion exchange capacities more precisely quantify charges at a sorbent's surface at specified pH than commonly used O/C ratios, total acidity or pH_{pzc} , they are yet rare to find in literature. In addition, an inclusion of appropriate descriptors for ionic PMOCs may be required as the current model applies Abraham parameters for uncharged compounds only (Abraham and Zhao, 2004; Zhang et al., 2020; Zhao et al., 2019). Involvement of ionization degrees $\text{A}^- \%$ and $\text{B}^+ \%$ solely might not fully solve the problem as implied by the distorted predicted trends. Finally, comprehensive characterization of the

sorbents beyond ion exchange properties may be useful for updating prediction models. Nevertheless, a compromise between practical applicability (easily approachable AC characteristics which can be potentially offered by AC suppliers) and precision of prediction is certainly required.

4. Conclusion

In the present study, surface chemistry of AC is identified as an important factor for adsorption performance especially towards ionic and ionizable PMOCs. Surface-defunctionalized ACF was found to promise the widest application potential to adsorb neutral, anionic and cationic PMOCs among three tested ACFs. The defunctionalization creates a rather hydrophobic carbon surface carrying positively charged sites which specifically improves the adsorption of anionic PMOCs, while benefiting the adsorption of all probed PMOCs including the studied quaternary amines. Therefore, surface defunctionalization can work as a universal strategy to facilitate the removal of a wide range of diverse PMOCs simultaneously meanwhile to extend fixed-bed adsorber operation times or reduce required dosage of powdered AC in WWTPs.

In contrast, surface oxidation of AC as a means to increase density of negative charges results in higher surface polarity which is clearly detrimental for adsorption of *p*-TSA, *p*-TsO⁻ and TPA⁺ due to enhanced competitive adsorption of water molecules to AC surface. However, it selectively enhanced the adsorption of BTMA⁺, i.e., the probed cationic PMOC with the smallest number of carbon atoms and the lowest log *D*. It is thus tentatively suggested that a threshold limit in the size of the hydrophobic part of cationic PMOCs exists, below which oxidized AC surfaces can benefit their adsorption due to intensified electrostatic attraction.

Our work further demonstrates that the challenges in prognosis of the complicated PMOC sorption behaviors on AC sorbents are not fully conquered by the state-of-the-art prediction tools, which evidently underestimates the impact of sorbent surface chemistry. Our findings alert that standardized quantitative parameters describing AC surface chemistry are needed which should be commonly reported in scientific studies and finally also in product sheets by AC producers. Such parameters can be applied as input for the improvement of sorption prediction models for newly emerging PMOCs. In this respect, ion exchange capacity which quantifies sorbent surface charges at specified pH is recommended as a meaningful parameter.

Acknowledgement:

We acknowledge the funding by Deutsche Forschungsgemeinschaft GE 3029/1-1 and the funding within the PhD-college STROMER of Thematic Area Environmental Engineering and Biotechnology of UFZ. We acknowledge Dr. Marcus Lange, Dr. Jens Möllmer, Dr. Hans Uhlig at Institut für Nichtklassische Chemie e.V. (INC), Leipzig, for CO₂ adsorption measurement; M.Sc. Andrea Prager at Leibniz Institute of Surface Engineering (IOM), Leipzig, for XPS determination; Dr. Ulf Roland and Dr. Frank Holzer for the ATR-FTIR measurement; Dr. Gabriel Sigmund at University of Vienna for fruitful discussions; and B.Sc. Ruonan Qin for assisting the work as an internship student on the adsorption of MTBE. We are thankful for the use of SEM at the Centre for Chemical Microscopy (ProVIS) at UFZ, which is supported by European Regional Development Funds (EFRE-Europe funds Saxony) and the Helmholtz Association.

References

- Abraham M.H., Zhao Y.H., 2004. Determination of solvation descriptors for ionic species: hydrogen bond acidity and basicity. *J. Org. Chem.* 69, 4677-4685.
- Aljerf L., 2018. High-efficiency extraction of bromocresol purple dye and heavy metals as chromium from industrial effluent by adsorption onto a modified surface of zeolite: kinetics and equilibrium study. *J. Environ. Manage.* 225, 120-132.
- Allothman Z., 2012. A review: fundamental aspects of silicate mesoporous materials. *Materials* 5, 2874-2902.
- Arp H.P.H., Brown T.N., Berger U., Hale S.E., 2017. Ranking REACH registered neutral, ionizable and ionic organic chemicals based on their aquatic persistency and mobility. *Environ. Sci.: Process. Impacts.* 19, 939-955.
- Arp H.P.H., Hale S.E., 2019. REACH: Improvement of guidance and methods for the identification and assessment of PMT/vPvM substances, Umweltbundesamt, <https://www.umweltbundesamt.de/publikationen/reach-improvement-of-guidance-methods-for-the> (accessed 1 June 2021).
- Atwood J.L., Steed J.W., 2004. *Encyclopedia of Supramolecular Chemistry Vol 1*, CRC Press, New York.
- Babić B.M., Milonjić S.K., Polovina M.J., Kaludierović B.V., 1999. Point of zero charge and intrinsic equilibrium constants of activated carbon cloth. *Carbon* 37, 477-481.
- Bayram E., Ayranci E., 2011. A systematic study on the changes in properties of an activated carbon cloth upon polarization. *Electrochim. Acta* 56, 2184-2189.
- Brooke D., Footitt A., Nwaogu T.A., 2004. Environmental risk evaluation report: Perfluorooctanesulphonate (PFOS) https://www.gov.uk/government/uploads/system/uploads/attachment_data/file/290857/scho1009brbl-e-e.pdf (accessed 1 June 2021).
- Brown M.A., Goel A., Abbas Z., 2016. Effect of electrolyte concentration on the Stern layer thickness at a charged interface. *Angew. Chem. Int. Ed.* 55, 3790-3794.
- Davarpanah M., Ahmadpour A., Rohani-Bastami T., Dabir H., 2015. Synthesis and application of diethanolamine-functionalized polystyrene as a new sorbent for the removal of p-toluenesulfonic acid from aqueous solution. *J. Ind. Eng. Chem.* 30, 281-288.
- Decrey L., Bonvin F., Bonvin C., Bonvin E., Kohn T., 2020. Removal of trace organic contaminants from wastewater by superfine powdered activated carbon (SPAC) is neither affected by SPAC dispersal nor coagulation. *Water Res.* 185, 116302.

Delpeux-Ouldriane S., Gineys M., Cohaut N., Béguin F., 2015. The role played by local pH and pore size distribution in the electrochemical regeneration of carbon fabrics loaded with bentazon. *Carbon* 94, 816-825.

Duman O., Ayranci E., 2010. Adsorptive removal of cationic surfactants from aqueous solutions onto high-area activated carbon cloth monitored by in situ UV spectroscopy. *J. Hazard. Mater.* 174, 359-367.

ECETOC, 2013. Environmental exposure assessment of ionizable organic compounds - technical report No. 123. European Centre for Ecotoxicology and Toxicology of Chemicals, Brussels. <https://www.ecetoc.org/publication/tr-123-environmental-risk-assessment-of-ionisable-compounds/> (accessed 1 June 2021).

Endo S., Goss K.-U., 2014. Applications of polyparameter linear free energy relationships in environmental chemistry. *Environ. Sci. Technol.* 48, 12477-12491.

EPA, 2020. United States Environmental Protection Agency: Drinking water treatment technology unit cost models and overview of technologies <https://www.epa.gov/sdwa/drinking-water-treatment-technology-unit-cost-models-and-overview-technologies> (accessed 16 April 2021).

Farré M.I., Pérez S., Kantiani L., Barceló D., 2008. Fate and toxicity of emerging pollutants, their metabolites and transformation products in the aquatic environment. *TrAC Trends Anal. Chem.* 27, 991-1007.

Fent K., Weston A.A., Caminada D., 2006. Ecotoxicology of human pharmaceuticals. *Aquat. Toxicol.* 76, 122-159.

Ferrari B.t., Paxéus N., Giudice R.L., Pollio A., Garric J., 2003. Ecotoxicological impact of pharmaceuticals found in treated wastewaters: study of carbamazepine, clofibric acid, and diclofenac. *Ecotoxicol. Environ. Saf.* 55, 359-370.

Goss K.-U., 2008. The pKa values of PFOA and other highly fluorinated carboxylic acids. *Environ. Sci. Technol.* 42, 456-458.

Guthrie J.P., 1978. Hydrolysis of esters of oxy acids: pKa values for strong acids; Brønsted relationship for attack of water at methyl; free energies of hydrolysis of esters of oxy acids; and a linear relationship between free energy of hydrolysis and pKa holding over a range of 20 pK units. *Can. J. Chem.* 56, 2342-2354.

Hotová G., Slovák V., Zelenka T., Maršálek R., Parchaňská A., 2020. The role of the oxygen functional groups in adsorption of copper (II) on carbon surface. *Sci. Total Environ.* 711, 135436.

Kah M., Sigmund G., Xiao F., Hofmann T., 2017. Sorption of ionizable and ionic organic compounds to biochar, activated carbon and other carbonaceous materials. *Water Res.* 124, 673-692.

- Lee K.J., Miyawaki J., Shiratori N., Yoon S.-H., Jang J., 2013. Toward an effective adsorbent for polar pollutants: formaldehyde adsorption by activated carbon. *J. Hazard. Mater.* 260, 82-88.
- Li L., Quinlivan P.A., Knappe D.R.U., 2002. Effects of activated carbon surface chemistry and pore structure on the adsorption of organic contaminants from aqueous solution. *Carbon* 40, 2085-2100.
- Li X., Pignatello J.J., Wang Y., Xing B., 2013. New insight into adsorption mechanism of ionizable compounds on carbon nanotubes. *Environ. Sci. Technol.* 47, 8334-8341.
- Liu Y., 2009. Is the free energy change of adsorption correctly calculated? *J. Chem. Eng. Data* 54, 1981-1985.
- Loos R., Carvalho R., António D.C., Comero S., Locoro G., Tavazzi S., et al., 2013. EU-wide monitoring survey on emerging polar organic contaminants in wastewater treatment plant effluents. *Water Res.* 47, 6475-6487.
- Mailler R., Gasperi J., Coquet Y., Derome C., Buleté A., Vulliet E., et al., 2016. Removal of emerging micropollutants from wastewater by activated carbon adsorption: experimental study of different activated carbons and factors influencing the adsorption of micropollutants in wastewater. *J. Environ. Chem. Eng.* 4, 1102-1109.
- Messori L., Casini A., Gabbiani C., Sorace L., Muniz-Miranda M., Zatta P., 2007. Unravelling the chemical nature of copper cuprizone. *Dalton Trans.*, 2112-2114.
- Qi Y., Jin X., Yu C., Wang Y., Yang L., Li Y., 2013. A novel chelating resin containing high levels of sulfamine group: preparation and its adsorption characteristics towards p-toluenesulfonic acid and Hg(II). *Chem. Eng. J.* 233, 315-322.
- Reemtsma T., Berger U., Arp H.P.H., Gallard H., Knepper T.P., Neumann M., et al., 2016. Mind the gap: persistent and mobile organic compounds—water contaminants that slip through. *Environ. Sci. Technol.* 50, 10308-10315.
- Reemtsma T., Weiss S., Mueller J., Petrovic M., González S., Barcelo D., et al., 2006. Polar pollutants entry into the water cycle by municipal wastewater: a european perspective. *Environ. Sci. Technol.* 40, 5451-5458.
- Saeidi N., Kopinke F.-D., Georgi A., 2020a. Understanding the effect of carbon surface chemistry on adsorption of perfluorinated alkyl substances. *Chem. Eng. J.* 381, 122689.
- Saeidi N., Kopinke F.-D., Georgi A., 2020b. What is specific in adsorption of perfluoroalkyl acids on carbon materials? *Chemosphere*, 128520.
- Schulze S., Sättler D., Neumann M., Arp H.P.H., Reemtsma T., Berger U., 2018. Using REACH registration data to rank the environmental emission potential of persistent and mobile organic chemicals. *Sci. Total Environ.* 625, 1122-1128.

- Schulze S., Zahn D., Montes R., Rodil R., Quintana J.B., Knepper T.P., et al., 2019. Occurrence of emerging persistent and mobile organic contaminants in European water samples. *Water Res.* 153, 80-90.
- Schwarzenbach R.P., Gschwend P.M., Imboden D.M., 1993. *Environmental Organic Chemistry*, John Wiley & Sons, Inc., New York.
- Sergeant E.P., Dempsey B., 1979. Ionisation constants of organic acids in aqueous solution. IUPAC chemical data series No. 23, Pergamon Press, New York.
- Sigmund G., Gharasoo M., Hüffer T., Hofmann T., 2020a. Comment on predicting aqueous adsorption of organic compounds onto biochars, carbon nanotubes, granular activated carbons and resins with machine learning. *Environ. Sci. Technol.* 54, 11636-11637.
- Sigmund G., Gharasoo M., Hüffer T., Hofmann T., 2020b. Deep learning neural network approach for predicting the sorption of ionizable and polar organic pollutants to a wide range of carbonaceous materials. *Environ. Sci. Technol.* 54, 4583–4591.
- Sinclair C.J., Boxall A.B.A., 2003. Assessing the ecotoxicity of pesticide transformation products. *Environ. Sci. Technol.* 37, 4617-4625.
- Sing K.S.W., Everett D.H., Haul R.A.W., Moscou L., Pierotti R.A., Rouquerol J., et al., 1985. Reporting physisorption data for gas/solid systems with special reference to the determination of surface area and porosity (recommendations 1984). *Pure Appl. Chem.* 57, 603-619.
- Sophia A.C., Lima E.C., 2018. Removal of emerging contaminants from the environment by adsorption. *Ecotoxicol. Environ. Saf.* 150, 1-17.
- Strelko V., Malik D.J., Streat M., 2002. Characterisation of the surface of oxidised carbon adsorbents. *Carbon* 40, 95-104.
- Tamai H., Kunihiro M., Yasuda H., 2004. Adsorption of tetraalkylammonium ions on microporous and mesoporous activated carbons prepared from vinylidene chloride copolymer. *J. Colloid Interface Sci.* 275, 44-47.
- Teixidó M., Pignatello J.J., Beltrán J.L., Granados M., Peccia J., 2011. Speciation of the ionizable antibiotic sulfamethazine on black carbon (biochar). *Environ. Sci. Technol.* 45, 10020-10027.
- Teychene B., Chi F., Chokki J., Darracq G., Baron J., Joyeux M., et al., 2020. Investigation of polar mobile organic compounds (PMOC) removal by reverse osmosis and nanofiltration: rejection mechanism modelling using decision tree. *Water Supply* 20, 975-983.
- Thomaidi V.S., Stasinakis A.S., Borova V.L., Thomaidis N.S., 2015. Is there a risk for the aquatic environment due to the existence of emerging organic contaminants in treated domestic wastewater? Greece as a case-study. *J. Hazard. Mater.* 283, 740-747.

- Tran H.N., You S.-J., Hosseini-Bandegharai A., Chao H.-P., 2017. Mistakes and inconsistencies regarding adsorption of contaminants from aqueous solutions: a critical review. *Water Res.* 120, 88-116.
- Ulrich N., Endo S., Brown T.N., Watanabe N., Bronner G., Abraham M.H., et al., 2017. UFZ-LSER Database v 3.2 <http://www.ufz.de/lserd> (accessed 16 April 2021).
- Vogel M., Kopinke F.-D., Mackenzie K., 2019. Acceleration of microiron-based dechlorination in water by contact with fibrous activated carbon. *Sci. Total Environ.* 660, 1274-1282.
- Watson J., 1999. *Separation Methods for Waste and Environmental Applications*, Marcel Dekker, New York.
- Wellen B.A., Lach E.A., Allen H.C., 2017. Surface pKa of octanoic, nonanoic, and decanoic fatty acids at the air–water interface: applications to atmospheric aerosol chemistry. *Phys. Chem. Chem. Phys.* 19, 26551-26558.
- Wu T., Cai X., Tan S., Li H., Liu J., Yang W., 2011. Adsorption characteristics of acrylonitrile, p-toluenesulfonic acid, 1-naphthalenesulfonic acid and methyl blue on graphene in aqueous solutions. *Chem. Eng. J.* 173, 144-149.
- Xiao F., Pignatello J.J., 2014. Effect of adsorption nonlinearity on the pH–adsorption profile of ionizable organic compounds. *Langmuir* 30, 1994-2001.
- Xiao F., Pignatello J.J., 2016. Effects of post-pyrolysis air oxidation of biomass chars on adsorption of neutral and ionizable compounds. *Environ. Sci. Technol.* 50, 6276-6283.
- Xiao J.-X., Zhang Y., Wang C., Zhang J., Wang C.-M., Bao Y.-X., et al., 2005. Adsorption of cationic–anionic surfactant mixtures on activated carbon. *Carbon* 43, 1032-1038.
- Yang W., 2019, *Electrochemical Advanced Oxidation Processes for Emerging Organic Contaminants Removal with Graphene-based Modified Carbon Felt Electrode*. PhD thesis.
- Zelazny L.W., He L., Vanwormhoudt A., 1996. Charge Analysis of Soils and Anion Exchange. *Methods of Soil Analysis: Part 3 Chemical Methods*, 5.3. Soil Science Society of America, Inc., American Society of Agronomy, Inc., Madison, pp. 1231-1253.
- Zhang K., Zhong S., Zhang H., 2020. Predicting aqueous adsorption of organic compounds onto biochars, carbon nanotubes, granular activated carbons and resins with machine learning. *Environ. Sci. Technol.* 54, 7008-7018.
- Zhao H., Qian L., Guan X., Wu D., Zhao G., 2016. Continuous bulk FeCuC aerogel with ultradispersed metal nanoparticles: an efficient 3D heterogeneous electro-Fenton cathode over a wide range of pH 3–9. *Environ. Sci. Technol.* 50, 5225-5233.
- Zhao Y., Lin S., Choi J.-W., Bediako J.K., Song M.-H., Kim J.-A., et al., 2019. Prediction of adsorption properties for ionic and neutral pharmaceuticals and pharmaceutical intermediates on activated charcoal from aqueous solution via LFER model. *Chem. Eng. J.* 362, 199-206.

Zhi Y., Liu J., 2016. Surface modification of activated carbon for enhanced adsorption of perfluoroalkyl acids from aqueous solutions. *Chemosphere* 144, 1224-1232.

Zhou J.-H., Sui Z.-J., Zhu J., Li P., Chen D., Dai Y.-C., et al., 2007. Characterization of surface oxygen complexes on carbon nanofibers by TPD, XPS and FT-IR. *Carbon* 45, 785-796.

Figures:

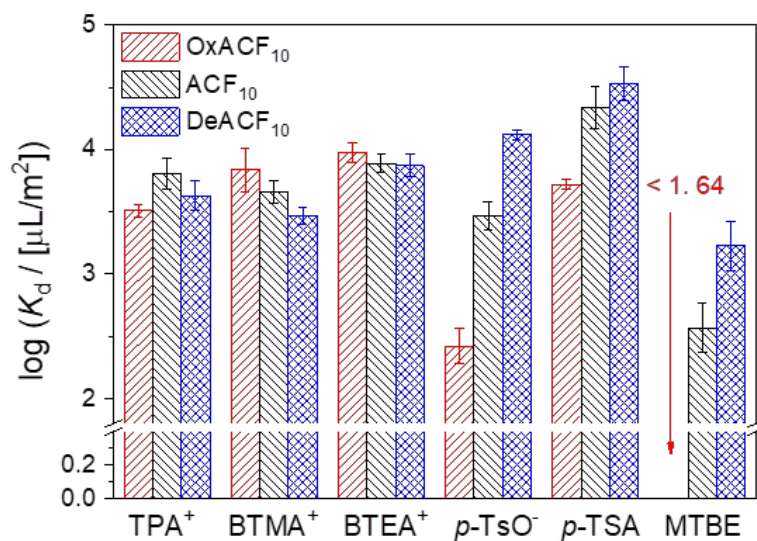


Fig. 1: Log K_d on ACFs for selected PMOCs at $c_e = 20 \mu\text{M}$ in 10 mM Na_2SO_4 solution at pH 7 at 20 °C. These values were calculated from the corresponding Freundlich isotherm parameters. The error bars of log K_d are calculated from the errors in K_F and n obtained from the regression analyses of the Freundlich linear fittings.

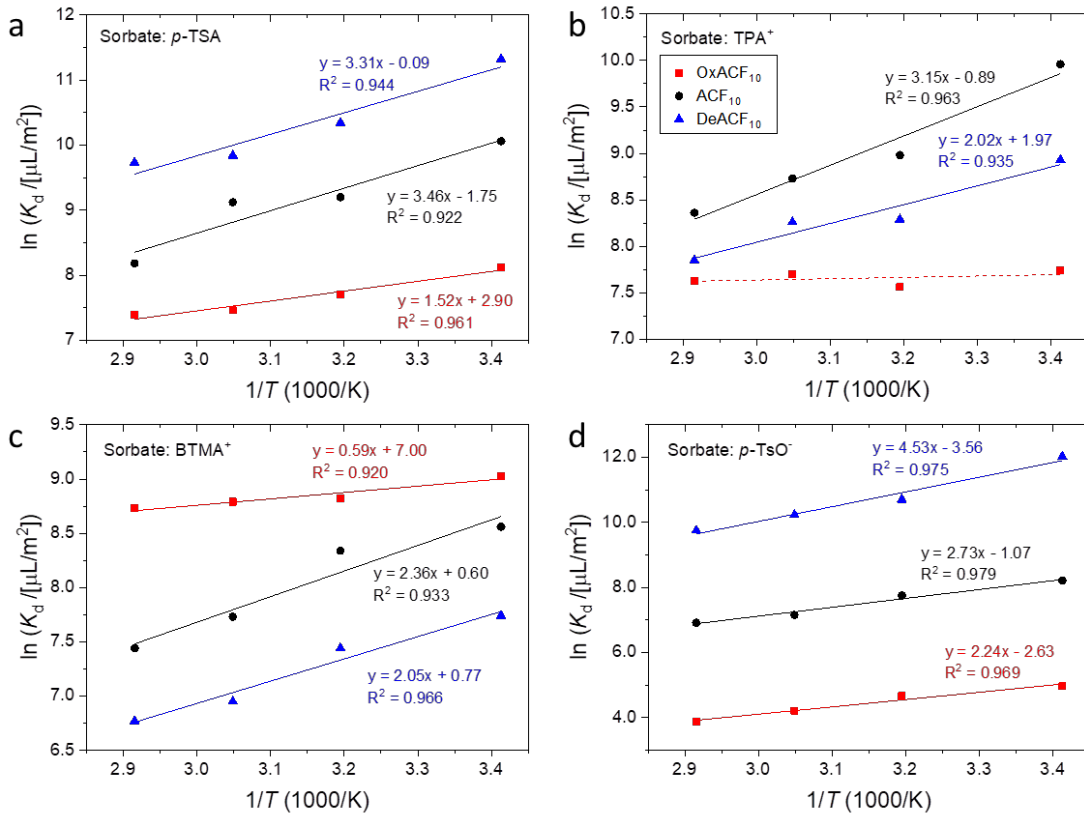


Fig. 2: Linear fittings of $\ln K_d$ vs. ($1/T$) for (a) *p*-TSA, (b) TPA⁺, (c) BTMA⁺ and (d) *p*-TsO⁻ in 10 mM Na₂SO₄ at pH 7. The initial concentration of dissolved sorbate was set at 20 mg/L. The experimental conditions (details given in SI) were selected giving $q \leq \frac{1}{2} q_{\max}$.

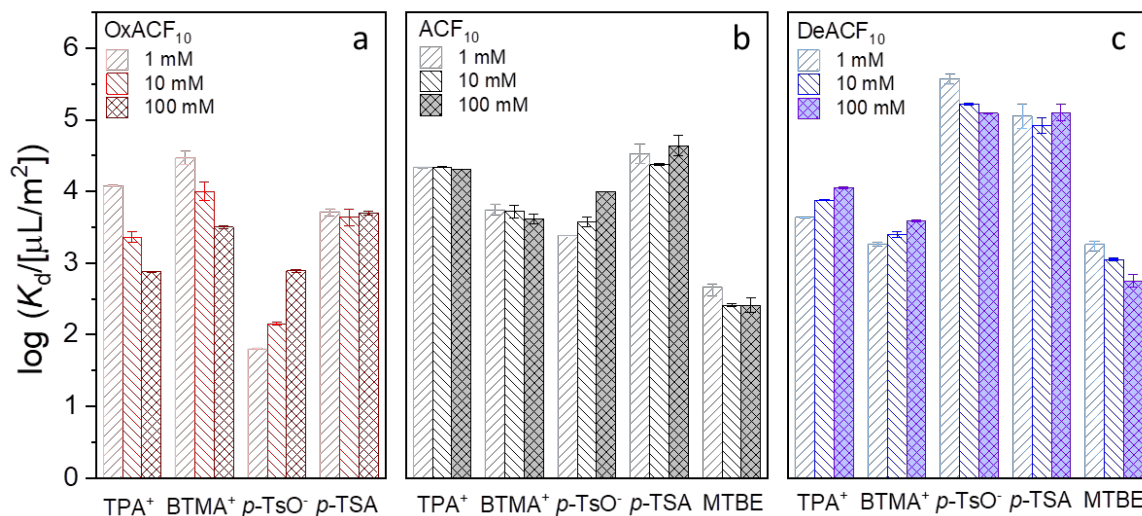


Fig. 3: The effect of electrolyte solution concentration on the adsorption of selected compounds on (a) OxACF₁₀, (b) ACF₁₀ and (c) DeACF₁₀ in Na₂SO₄ solution at pH 7. The experimental conditions (details given in SI) were selected to ensure $q \leq 2/3 q_{\text{max}}$. The error bars are standard deviations of the single values from duplicate experiments with triplicate measurements each.

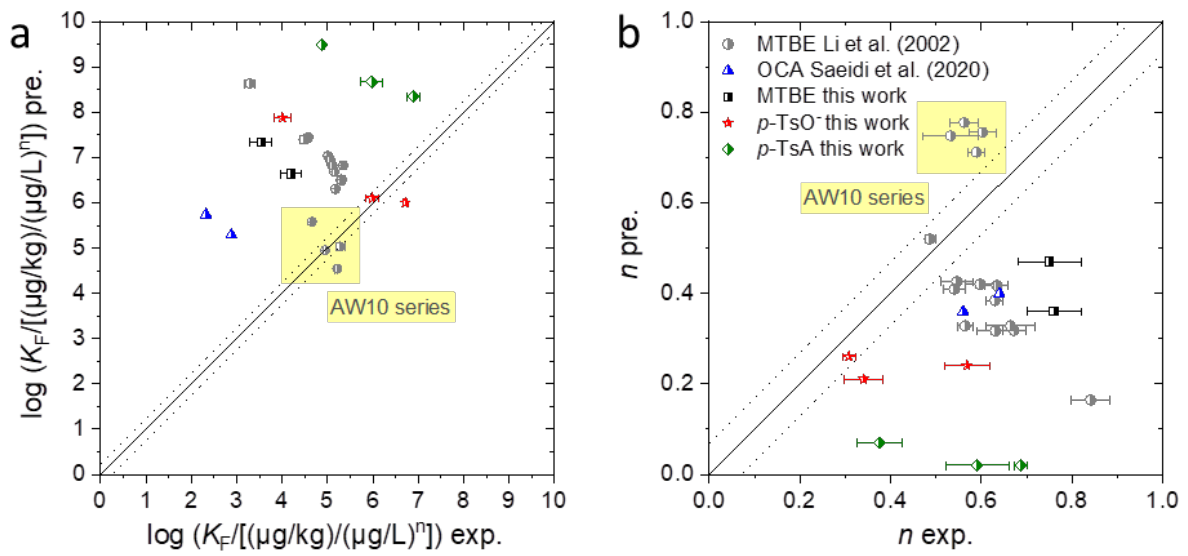


Fig. 4: Comparison of experimentally derived and predicted Freundlich isotherm parameters (a) $\log K_F$ and (b) n by the model of Sigmund et al. (2020b). K_F are given in $(\mu\text{g/kg})/(\mu\text{g/L})^n$ as used also by Sigmund et al. (2020b). Error bars are obtained from the regression analyses of experimentally derived Freundlich fittings. Functions $y = x$ for both $\log K_F$ and n are shown by the black solid lines. Typical expected deviation ranges for $\log K_F$ and n are marked with dashed lines.

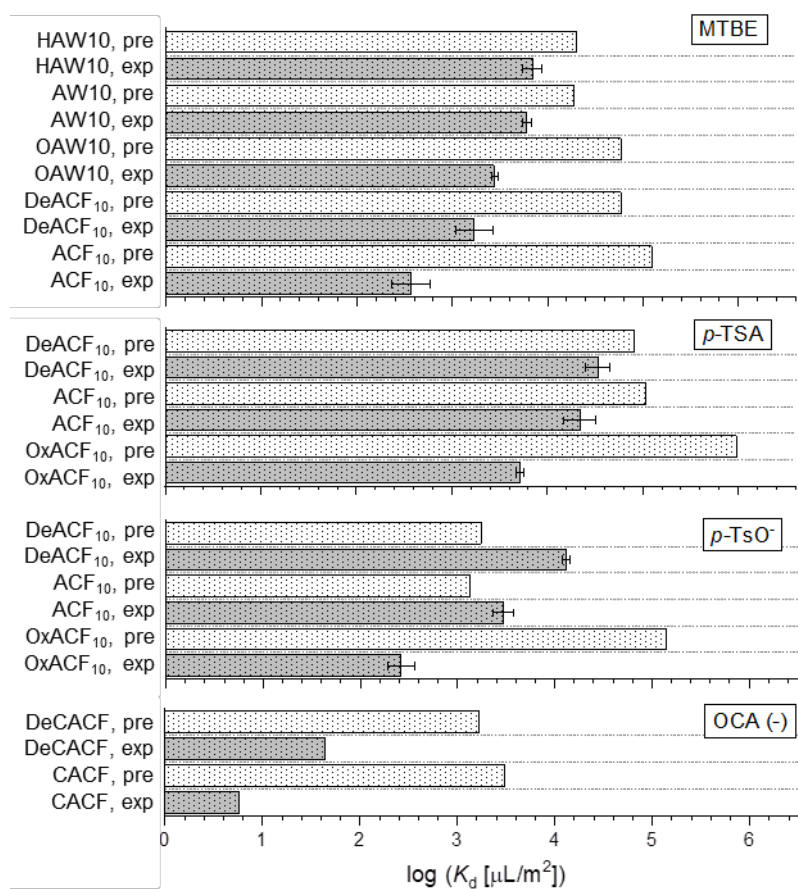


Fig. 5: Experimentally derived and predicted $\log K_d$ of MTBE, p -TSA, p -TsO⁻ and OCA (-) at $c_e = 20 \mu\text{M}$ on various ACFs in 10 mM Na₂SO₄ solution at pH 7. Log K_d and error bars were obtained as for Fig. 1. DeCACF contains a lower O-content and a more hydrophobic surface with a higher delocalized π -electron density than CACF (Saeidi et al., 2020b).

Tables:

Table 1: Chemical properties of untreated ACF₁₀ and surface-modified OxACF₁₀ and DeACF₁₀.

Sample	pH _{PZC}	CEC (μmol/m ²)	AEC (μmol/m ²)	C wt%	H wt%	O wt% ^a	N wt%
OxACF ₁₀	2.4 ± 0.1	1.0	0.0087	78.5	0.3	18.1	2.7
ACF ₁₀	5.7 ± 0.2	0.040	0.025	87.7	0.3	9.9	1.8
DeACF ₁₀	10.2 ± 0.2	≤ 0.010	0.23	93.4	0.4	4.3	0.9

^a Calculated from mass balance according to O wt% = 100% – C wt% – H wt% – N wt% – ash wt%.

Table 2: Textural properties of ACF₁₀, OxACF₁₀, and DeACF₁₀. V_t = total pore volume; V_{meso} = mesopore volume; $V_{\text{micro}, \varnothing < 1 \text{ nm}}$ and $V_{\text{micro}, \varnothing = 1-2 \text{ nm}}$ = pore volume of micropores with $\varnothing < 1 \text{ nm}$ and $\varnothing = 1-2 \text{ nm}$.

Sample	S_{BET} (m ² /g) ^a	V_t (cm ³ /g) ^b	$V_{\text{micro}, \varnothing < 1 \text{ nm}}$ (cm ³ /g) ^b	$V_{\text{micro}, \varnothing = 1-2 \text{ nm}}$ (cm ³ /g) ^b	V_{meso} (cm ³ /g) ^b
OxACF ₁₀	1100	0.51	0.16	0.31	0.04
ACF ₁₀	1500	0.57	0.14	0.39	0.04
DeACF ₁₀	1400	0.73	0.08	0.58	0.07

^a Determined by N₂ adsorption/desorption up to $p/p_0 = 0.99$. ^b Determined by CO₂ adsorption.

Table 3: Freundlich and Langmuir isotherm parameters for adsorption of six PMOCs on three ACFs in 10 mM Na₂SO₄ solution at pH 7, 20°C.

Sorbate	ACF sorbent	Freundlich			Langmuir		
		$K_F (10^{-3} (\mu\text{mol}/\text{m}^2)/(\mu\text{mol}/\text{L})^n)$	n	R^2	$q_{\text{max}} (\mu\text{mol}/\text{m}^2)$	$K_L (\text{L}/\mu\text{mol})$	R^2
TPA ⁺	OxACF ₁₀	18	0.42	0.995	0.18	0.031	0.986
	ACF ₁₀	35	0.44	0.970	0.16	0.11	0.974
	DeACF ₁₀	28	0.37	0.958	0.13	0.11	0.996
BTMA ⁺	OxACF ₁₀	19	0.67	0.998	0.53	0.018	0.969
	ACF ₁₀	34	0.33	0.974	0.23	0.035	0.941
	DeACF ₁₀	12	0.54	0.995	0.22	0.016	0.992
BTEA ⁺	OxACF ₁₀	85	0.27	0.963	0.36	0.087	0.979
	ACF ₁₀	68	0.28	0.977	0.28	0.081	0.982
	DeACF ₁₀	68	0.26	0.934	0.30	0.060	0.976
<i>p</i> -TsO ⁻	OxACF ₁₀	0.95	0.57	0.970	0.025	0.013	0.916
	ACF ₁₀	21	0.34	0.939	0.11	0.084	0.993
	DeACF ₁₀	100	0.31	0.994	0.38	0.14	1.000
<i>p</i> -TSA	OxACF ₁₀	13	0.69	0.999	0.36	0.024	0.944
	ACF ₁₀	75	0.59	0.947	1.0	0.037	0.997
	DeACF ₁₀	220	0.38	0.935	1.3	0.079	0.984
MTBE	OxACF ₁₀	n.d. ^a	n.d. ^a	n.d. ^a	n.d. ^a	n.d. ^a	n.d. ^a
	ACF ₁₀	0.77	0.76	0.980	0.098	0.0037	0.854
	DeACF ₁₀	3.6	0.75	0.977	0.16	0.014	0.974

^a OxACF₁₀ has a very low adsorption to MTBE (no significant depletion up to ACF dosage of 5 g/L).